J Therm Anal Calorim (2012) 110:793–798
DOI 10.1007/s10973-011-1992-9

Crystallization behavior of Mg–Cu–Y amorphous alloy

Musa Gogebakan · Ibrahim Karteri · Baris Avar · Celal Kursun

Received: 30 June 2011 / Accepted: 11 October 2011 / Published online: 2 November 2011

Abstract Amorphous $Mg_{61}Cu_{24}Y_{15}$ ribbons were manufactured by melt-spinning at wheel speeds in the range 5–20 ms^{-1}. The crystallization behavior of amorphous ribbons was investigated by a combination of differential scanning calorimetry (DSC) and X-ray diffractometry. DSC measurements showed that the amorphous ribbons exhibit distinct glass transition temperature and wide supercooled liquid region before crystallization. During continuous heating three exothermic peaks and two endothermic peaks were observed. The characteristic thermodynamic parameters such as T_g, T_x, ΔT_x, and T_{rg} are around 432–439, 478–485, 46–54 K, and 0.55–0.56, respectively. Isothermal annealing DSC traces for this amorphous alloy, the first crystallization peak showed a clear incubation period and Avrami exponent was found to be 2.30–2.74, which indicate that the transformation reaction involved nucleation and three-dimensional diffusion controlled growth. Mechanical properties of the as-quenched and subsequently annealed ribbons were examined by Vickers microhardness (*HV*) measurements. Results showed that microhardness of the as-quenched ribbons were about 309 *HV*. However, the results also showed that microhardness of the rapidly solidified ribbons increases with the increasing temperature.

Keywords Magnesium alloys · Rapid solidification · Crystallization · Hardness measurement

M. Gogebakan · I. Karteri · B. Avar (✉) · C. Kursun
Department of Physics, Faculty of Arts and Sciences, Kahramanmaras Sutcu Imam University, Kahramanmaras 46100, Turkey
e-mail: barisavar@ksu.edu.tr

Introduction

Although magnesium and its alloys are the lightest materials, they suffer from low strength, low ductility, and poor corrosion resistance. Therefore, amorphous Mg-based alloys have been developed to improve tensile strength and corrosion resistance. Recently, new Mg-based amorphous alloys such as the Mg–TM–RE (TM = transition metal, RE = rare earth metal) systems with high tensile strength, good ductility and a wide supercooled liquid region have been obtained by using different techniques [1–5]. Since then, therefore, much attention has been paid to this subject. On the other hand, Mg-based amorphous and nanocrystalline materials are promising for hydrogen storage applications because of their high hydrogen storage capacity, lower specific weight, rich natural resource, and low cost. Therefore, the preparation, properties and application of Mg-based amorphous and nanocrystalline alloys have been a subject of growing interest in the field of alloy science. Although there have been previous studies of Mg–Cu–Y ternary alloys [6–9], there have been relatively little detailed study on their thermal properties, in particular the crystallization behavior, mechanism of crystallization, and crystallization activation energy. Differential scanning calorimeter (DSC) measurement shows that the amorphous $Mg_{61}Cu_{24}Y_{15}$ alloy exhibits distinct glass transition temperature and a wide supercooled liquid region before crystallization. Thus, the melt-spun $Mg_{61}Cu_{24}Y_{15}$ alloy is a nice example of amorphous sample for investigating its thermal properties. Another reason for the interest in the crystallization behavior of amorphous $Mg_{61}Cu_{24}Y_{15}$ alloy is the possibility to produce stable nanocrystalline microstructures with improving mechanical properties. In the present article, crystallization behavior of the rapidly solidified Mg–Cu–Y alloy with nominal composition of

$Mg_{61}Cu_{24}Y_{15}$ has been investigated by X-ray diffraction (XRD) and DSC techniques. The Vickers microhardness (*HV*) of the as-quenched and subsequently annealed ribbons was also examined to learn the variation of the mechanical properties as the phase contents change.

Experimental procedure

The master alloy with nominal composition of $Mg_{61}Cu_{24}Y_{15}$ (at.%) was prepared by melting of high purity Mg (99.90%), Cu (99.99%), and Y (98%) in an induction furnace under pure argon atmosphere. From the master alloy, the rapidly solidified ribbons were manufactured by using melt spinning with a wheel surface velocity of 5–20 ms^{-1}. The resulting melt-spun ribbons were typically 60–100 μm thick, 3–5 mm wide and up to several meters long. Crystallization behavior of amorphous ribbons was investigated by DSC (Perkin-Elmer Sapphire) using combination of continuous heating at heating rate of 5–40 K min^{-1}, and isothermal annealing at the temperatures in the range 453–463 K. Specimens of amorphous ribbon were also annealed at various temperatures from 423 to 650 K in the DSC at a heating rate of 20 K min^{-1} and cooled to room temperature. The structures of the as melt-spun and annealed ribbons were examined by XRD using Philips X'Pert PRO diffractometer with CuK_{α} radiation ($\lambda = 0.154$ nm) at 40 kV and 30 mA. The Vickers *HV* measurements of the as-quenched and subsequently annealed ribbons were performed using a Shimadzu HMV-2, with a load of 0.98 N for 10 s. An average of 10 readings at different places in the blade was taken for each specimen.

Results and discussion

Figure 1 shows XRD patterns of the as melt-spun $Mg_{61}Cu_{24}Y_{15}$ alloys prepared using wheel surface velocity of 5–20 ms^{-1}. The XRD patterns consist of broad diffraction peaks in the 2θ range of 30–45 deg, which is characteristic of an amorphous structure without the evidence of any crystalline peaks within XRD resolution. The formation of the amorphous phase even at a low wheel speed of 5 ms^{-1} in these alloys suggests that they have good glass forming ability.

Crystallization behavior of the rapidly solidified $Mg_{61}Cu_{24}Y_{15}$ alloys is determined using the DSC during continuous heating at a heating rate of 20 K min^{-1} and the corresponding DSC traces were shown in Fig. 2. As seen in Fig. 2, the melt-spun $Mg_{61}Cu_{24}Y_{15}$ alloys exhibit similar crystallization behavior starting with distinct glass transition temperature and a wide supercooled liquid region. All

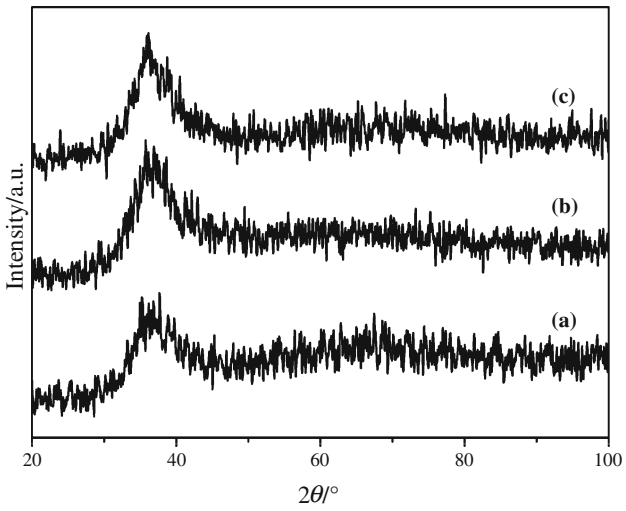

Fig. 1 XRDpatterns of the amorphous $Mg_{61}Cu_{24}Y_{15}$ alloy prepared using different wheel speeds: (*a*) 5 ms^{-1}, (*b*) 10 ms^{-1}, and (*c*) 20 ms^{-1}

the samples exhibit three obvious exothermic reactions because of crystallization. Similar crystallization behavior was reported by Linderoth et al. [9] for $Mg_{60}Cu_{30}Y_{10}$ alloy and by Cheng et al. [10] for $Mg_{65}Cu_{25}Y_{10}$ alloy. Glass transition temperature, T_g, crystallization temperature, T_x, supercooled liquid region, ΔT_x ($\Delta T_x = T_x - T_g$), and three crystallization peak temperatures, T_{p1}, T_{p2}, T_{p3} are listed in Table 1. However, the thermal stability of an amorphous alloy can be correlated to its crystallization temperature T_x, glass transition temperature T_g, and the activation energy of crystallization *E*. Usually, the higher T_x, T_g, and *E*, the more stable amorphous phase. On the other hand, the glass transition behavior for amorphous alloys is of technological and scientific importance, because the glass transition

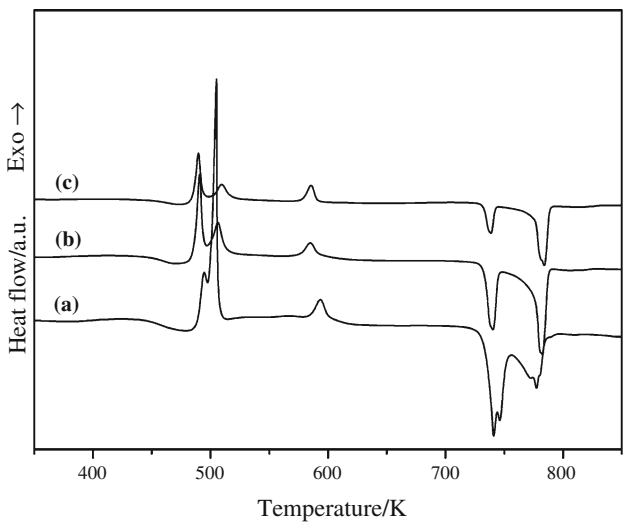

Fig. 2 Continuous DSC traces from the amorphous $Mg_{61}Cu_{24}Y_{15}$ alloy manufactured using different wheel speeds: (*a*) 5 ms^{-1}, (*b*) 10 ms^{-1}, and (*c*) 20 ms^{-1}

Table 1 Result of thermal analysis (T_g, T_x, T_p, T_m^{sol} and T_m^{liq}) and calculated parameters (ΔT_x, ΔT_m, and T_{rg})

Wheel speed/ms^{-1}	T_g/K	T_x/K	ΔT_x/K	T_{p1}/K	T_{p2}/K	T_{p3}/K	T_{m1}^{sol}/K	T_{m1}^{liq}/K	ΔT_{m1}/K	T_{m2}^{sol}/K	T_{m2}^{liq}/K	ΔT_{m2}/K	T_{rg}
5	439	485	46	494	504	593	726	753	27	757	785	28	0.56
10	435	482	47	490	506	584	727	747	20	751	789	38	0.55
20	432	478	54	489	509	585	728	743	15	748	790	42	0.55

reflects atomic transport and viscosity properties which are dominant factors in the glass forming ability of alloys and in the structural relaxation and thermal stability of the amorphous structure. However as shown in the Table 1, there is a trend of decreasing T_g and T_x with increasing melt-spun wheel speed. This suggests that in amorphous $Mg_{61}Cu_{24}Y_{15}$ alloy, the amorphous phase is less stable at higher melt-spun wheel speeds. Similar trend was reported by Murty and Hono [11].

The melting behavior of the $Mg_{61}Cu_{24}Y_{15}$ alloys is also determined using the DSC during continuous heating at a heating rate of 20 K min^{-1}. As seen in Fig. 2, continuous heating DSC traces of the melt-spun $Mg_{61}Cu_{24}Y_{15}$ alloys exhibit two endothermic reactions because of melting events. From the former report by Lu et al. [12], $Mg_{65}Cu_{25}Y_{10}$ alloys would exhibit a single endothermic peak with a narrow melting range of about 40 K, suggested that the alloy may be very close to the ternary eutectic composition. In the present study, the $Mg_{61}Cu_{24}Y_{15}$ alloys exhibit two melting events, indicating that the alloy is at off-eutectic composition. The onset melting temperatures, T_{m1}^{sol}andT_{m2}^{sol}, end melting temperatures, T_{m1}^{liq} and T_{m2}^{liq}, melting temperature intervals, ΔT_{m1} and ΔT_{m2} ($\Delta T_m = T_m^{liq} - T_m^{sol}$) for each endothermic reaction, and reduced glass transition temperature, T_{rg} ($T_{rg} = T_g/T_{m2}^{liq}$) are also listed in Table 1.

It is well known that the temperatures of the exothermic peaks depend on the heating rate and it is possible to obtain effective activation energy for crystallization by using Kissinger equation [13]:

$$\ln\left(\frac{T^2}{\beta}\right) = \left(\frac{E}{RT}\right) + A\,. \qquad (1)$$

where T is the peak temperature, β is the heating rate, E is the activation energy, R is the gas constant (8.314 J/mol K), and A is a constant. A plot of ln (T^2/β) versus ($1/T$) yield an approximate straight line with a slope of (E/R), then the E can be obtained from the slope. This type of analysis has previously been used for the determination of E for various amorphous alloys [9, 14, 15]. The activation energies calculated from the slope are presented in Table 2. As seen in Table 2, the calculated values of the overall activation energy for the first crystallization peaks compare reasonably well with the activation energies of 139–154 kJ mol^{-1} (1.44–1.6 eV) previously reported for $Mg_{65}Cu_{25}Y_{10}$ and $Mg_{60}Cu_{30}Y_{10}$ alloys [10, 15, 16].

Table 2 Activation energies E/kJ mol^{-1} for crystallization in $Mg_{61}Cu_{24}Y_{15}$ alloys prepared using different wheel speeds

Wheel speed/ms^{-1}	First peak/kJ mol^{-1}	Second peak/kJ mol^{-1}	Third peak/kJ mol^{-1}
5	156	189	163
10	145	197	174
20	142	190	158

However, the values of the activation energies for the first exothermic peaks are higher at lower melt-spun wheel speeds. The higher activation energy implies that the energy barrier for the glass-to-crystalline phase transformation is higher, and that the amorphous structure is more stable at temperatures lower than the crystallization temperature.

To obtain information about the mechanism of the crystallization reaction in the amorphous $Mg_{61}Cu_{24}Y_{15}$ alloy, an isothermal annealing study at different temperatures was carried out. Figures 3 and 4 show typical isothermal annealing DSC traces and corresponding transformation curves from the amorphous $Mg_{61}Cu_{24}Y_{15}$ alloy prepared at a wheel speed of 10 ms^{-1}. After a well-defined incubation time τ, the isothermal DSC curves reveal clearly an exothermic peak with smooth onset and sharper end. These bell-shaped curves are generally an

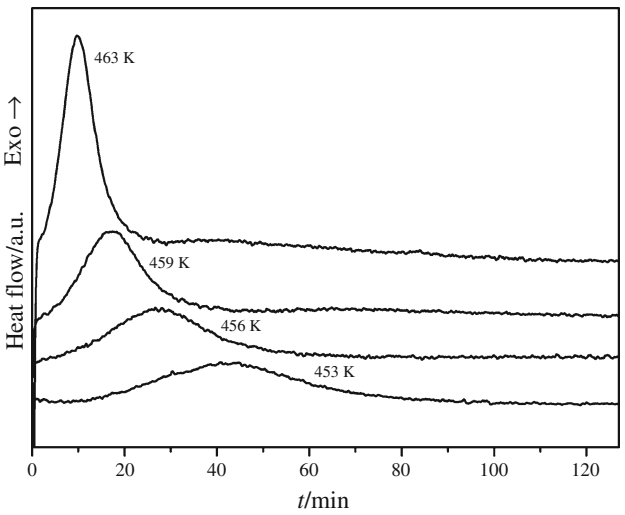

Fig. 3 DSC traces from the amorphous $Mg_{61}Cu_{24}Y_{15}$ alloy obtained during isothermal annealing at various temperatures

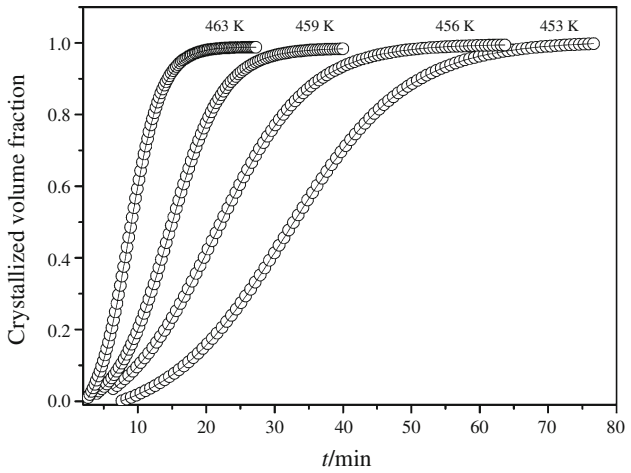

Fig. 4 Effect of annealing temperature on the rate of crystallization in the temperature range 453–463 K

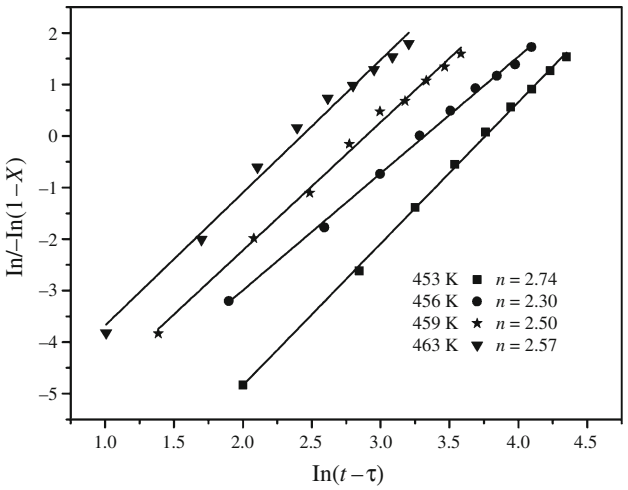

Fig. 5 Avrami plots for the amorphous $Mg_{61}Cu_{24}Y_{15}$ alloy

indication of nucleation and growth in a crystallization process, proving that the alloys are amorphous rather than nanocrystalline [17]. The crystallized volume fraction X, as a function of time at different isothermal annealing temperatures is shown in Fig. 4. The X was obtained by integrating the area underneath each DSC curve for various time increments between t_s and t_f which correspond to the start and finish times for the crystallization, respectively. As seen in Fig. 4, the sigmoid form of the obtained curves is the characteristic of the volumetric crystallization as such in other studies [15, 16, 18, 19].

Using the data obtained from the isothermal annealing DSC experiments, the transformation kinetics can be analyzed using Johnson-Mehl-Avrami (JMA) equation [20]:

$$X = 1 - \exp\{-[K\,(t-\tau)^n]\} \qquad (2)$$

where X is the fractional transformation at time t, n is the Avrami exponent depending on the nucleation and growth mechanism, τ is the incubation time, and K is the reaction rate constant. The Avrami exponent n is obtained from plots of $\ln[-\ln(1-X)]$ versus $\ln(t-\tau)$. The Avrami plots are shown in Fig. 5. The Avrami exponent n takes a value in the range 2.30–2.74, depending on the annealing temperature. An Avrami exponent with $n = 2.5$ is an indication that the transformation process could be taking place by continuous nucleation and three-dimensional diffusion controlled growth.

In order to identify the crystallization products, the melt-spun ribbons were heated in the DSC by heating rate of 20 K min^{-1} to temperatures in range 423–650 K. Fig. 6 shows the XRD patterns obtained from the amorphous $Mg_{61}Cu_{24}Y_{15}$ alloy (prepared at a wheel speed of 10 ms^{-1}) after heat treatments. The XRD patterns of $Mg_{61}Cu_{24}Y_{15}$ amorphous samples after annealing at temperatures from 423 to 480 i.e., before the first crystallization peak show only an amorphous phase. The first traces of crystallization were detected after heating to 500 K, which is just above the first crystallization peak in DSC, and all the peaks in the XRD pattern can be indexed as orthorhombic Mg_2Cu phases along with the amorphous phase. It can be concluded that in this alloy, the first crystallization peaks in DSC correspond to primary crystallization of the amorphous phase to precipitate Mg_2Cu phases. The XRD peaks of the Mg_2Cu remain during annealing of the alloy. After primary crystallization, heating up to 523 K, which is after the second exothermic peak in DSC, the samples are fully crystallized, and the main phases observed are Mg_2Cu, $Mg_{24}Y_5$, Cu_2Y, and Mg, they are marked by symbols on the Fig. 6. However, after annealing up to 650 K i.e., above the third exothermic peak in DSC, no new phases in the XRD traces were observed, and the intensity of the

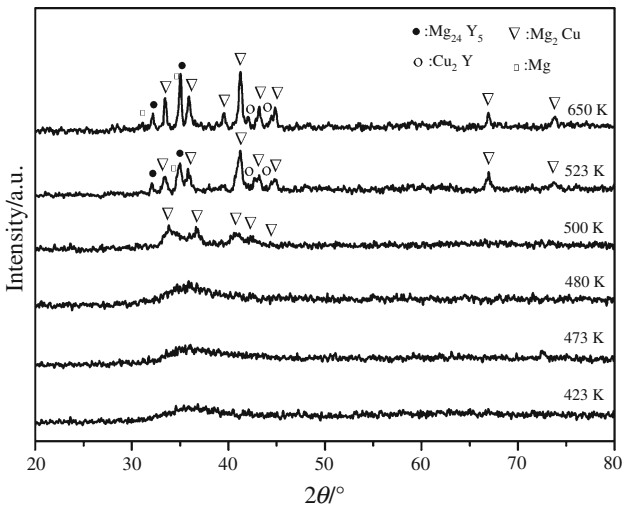

Fig. 6 XRD patterns from amorphous $Mg_{61}Cu_{24}Y_{15}$ alloy after annealed at different temperatures

Table 3 Results of *HV* measurements on as-quenched and subsequently annealed ribbons

Melt-spun ribbons (K)	Vickers microhardness (*HV*)	Structure
R.T*	309 ± 45	Amorphous
423	322 ± 47	Amorphous
473	347 ± 53	Amorphous
480	376 ± 65	Amorphous
500	411 ± 60	Crystalline
523	430 ± 55	Crystalline
650	435 ± 48	Crystalline

* Room temperature

present phases were increased. The diffraction pattern from the fully crystalline alloy contains several unidentified reflections, as reported previously [21]. Similar crystallization products were reported by Gun et al. [15] for amorphous Mg_{60} $Cu_{30}Y_{10}$ alloy, and Soubeyroux and Puech for $Mg_{58.5}Cu_{30.5}Y_{11}$ alloy [21].

Another goal of the present study was to examine the mechanical properties in as-quenched and annealed states of the rapidly solidified $Mg_{61}Cu_{24}Y_{15}$ alloy. The mechanical properties of the as-quenched and subsequently annealed ribbons were determined by Vickers *HV* measurements. The Vickers *HV* was calculated using the relation,

$$HV = \frac{2P\sin(\theta/2)}{d^2} = \frac{1.8544(P)}{d^2} \quad (3)$$

where P is the indentation force, d is the average diagonal length and 1.8544 is the geometrical factor for the diamond pyramid [22]. The Vickers *HV* values of as-quenched and annealed ribbons are summarized in Table 3, which indicates that Vickers *HV* increases through crystallization temperatures in range 423–650 K. The increase in *HV* values of ribbons annealed after 423–480 K corresponds to atomic rearrangement in the amorphous state (seen in Fig. 6). The highest *HV* value for the amorphous ribbons was found to be 376 ± 65 *HV* at 480 K, which is higher than about 100 *HV* for $Mg_{65}Cu_{25}Y_{10}$ obtained by Gang et al. [23] and for $Mg_{83}Ni_9Y_8$ obtained by Perez et al. [24]. However, during annealing up to 650 K, the *HV* values increase parallel to increasing volume fraction of crystalline phases. So, the highest *HV* value was found to be 435 ± 48 *HV* at 650 K for fully crystallized ribbon. These results are good agreement with other results [23–25].

Conclusions

In the present research, amorphous $Mg_{61}Cu_{24}Y_{15}$ ribbons were manufactured by melt-spinning at wheel speeds in the range 5–20 ms^{-1}. DSC measurements showed that the amorphous ribbons exhibit distinct glass transition temperature and wide supercooled liquid region before crystallization. During continuous heating three exothermic peaks because of crystallization and two endothermic peaks because of melting events were observed. The characteristic thermodynamic parameters such as T_g, T_x, ΔT_x, and T_{rg} are around 432–439, 478–485, 46–54 K, and 0.55–0.56, respectively. Activation energies for three crystallization peaks, determined by the Kissinger method, are around 142–156, 189–192, and 158–174 kJ mol^{-1}, respectively. The transformation kinetics were analyzed by JMA equation with an Avrami exponent of $n = 2.30$–2.74, corresponding continuous nucleation and three-dimensional diffusion controlled growth. For the $Mg_{61}Cu_{24}Y_{15}$ alloy, Mg_2Cu phase forms by primary crystallization process form the amorphous phase. Subsequent crystallization follows by decomposition of the residual amorphous phase into intermetallic compounds. The value of *HV* for melt-spun ribbons increased with an increasing value of crystallization temperature.

Acknowledgements We would like to thank Kahramanmaras Sutcu Imam University for financial support of the research program (Project No: 2010/3-11).

References

1. Kim SG, Inoue A, Masumoto T. High mechanical strengths of Mg–Ni–Y and Mg–Cu–Y amorphous-alloys with significant supercooled liquid region. Mater Trans JIM. 1990;31:929–34.
2. Inoue A, Kato A, Zhang T, Kim SG, Masumoto T. Mg–Cu–Y amorphous-alloys with high mechanical strengths produced by a metallic mold casting method. Mater Trans JIM. 1991;32:609–16.
3. Inoue A, Masumoto T. Production and properties of light-metal-based amorphous-alloys. Mater Sci Eng A. 1991;133:6–9.
4. Inoue A, Masumoto T. Mg-based amorphous-alloys. Mater Sci Eng A. 1993;173:1–8.
5. Busch R, Liu W, Johnson WL. Thermodynamics and kinetics of the $Mg_{65}Cu_{25}Y_{10}$ bulk metallic glass forming liquid. J Appl Phys. 1998;83:4134–41.
6. Madge SV, Greer AL. Effect of Ag addition on the glass-forming ability and thermal stability of Mg–Cu–Y alloys. Mater Sci Eng A. 2004;375:759–62.
7. Lee PY, Lo C, Jang JSC. Consolidation of mechanically alloyed $Mg_{49}Y_{15}Cu_{36}$ powders by vacuum hot pressing. J Alloys Comp. 2007;434:354–7.
8. Lee PY, Kao MC, Lin CK, Huang JC. Mg–Y–Cu bulk metallic glass prepared by mechanical alloying and vacuum hot-pressing. Intermetallics. 2006;14:994–9.
9. Linderoth S, Pryds NH, Ohnuma M, Pedersen AS, Eldrup M, Nishiyama N, Inoue A. On the stability and crystallisation of bulk amorphous Mg–Cu–Y–Al alloys. Mater Sci Eng A. 2001;304:656–9.
10. Cheng YT, Hung TH, Huang JC, Jang JSC, Tsao JA, Lee PY. Effects of partial replacement of Cu and Y by B in Mg–Cu–Y amorphous alloys. Intermetallics. 2006;14:866–70.
11. Murty BS, Hono K. Formation of nanocrystalline particles in glassy matrix in melt-spun Mg–Cu–Y based alloys. Mater Trans JIM. 2000;41:1538–44.

12. Lu ZP, Tan H, Li Y, Ng SC. The correlation between reduced glass transition temperature and glass forming ability of bulk metallic glasses. Scripta Mater. 2000;42:667–73.
13. Kissinger HE. Reaction kinetics in differential thermal analysis. Anal Chem. 1957;29:1702–6.
14. Patel AT, Pratap A. Kinetics of crystallization of $Zr_{52}Cu_{18}Ni_{14}Al_{10}Ti_6$ metallic glass. J Therm Anal Calorim. 2011; doi: 10.1007/s10973-011-1549-y.
15. Gun B, Laws KJ, Ferry M. Static and dynamic crystallization in Mg–Cu–Y bulk metallic glass. J Non-Cryst Solids. 2006;352: 3887–95.
16. Pryds N, Eldrup M, Pedersen AS. In: Proceedings of the 22nd Riso international symposium on materials science. Science of metastable and nanocrystalline alloys structure, properties and modelling. Roskilde, Denmark: Riso National Laboratory; 2001. p. 377–82.
17. Chen LC, Spaepen F. Analysis of calorimetric measurements of grain-growth. J Appl Phys. 1991;69:679–85.
18. Du YL, Li W, Deng YH, Xu F. Effects of gaseous hydrogenation on crystallization behavior of melt-spun $Mg_{63}Pr_{15}Ni_{22}$ amorphous ribbons. J Therm Anal Calorim. 2010;99:191–5.
19. Sidel SM, Santos FA, Gordo VO, Idalgo E, Monteiro AA, Moraes JCS, Yukimitu K. Avrami exponent of crystallization in tellurite glasses. J Therm Anal Calorim. 2011. doi:10.1007/s10973-011-1312-4.
20. Christian JW. The theory of transformations in metals and alloys, Part I. Oxford: Pergamon Press; 1957.
21. Soubeyroux JL, Puech S. Phases formation during heating of Mg–Cu–Ag–Y bulk metallic glasses. J Alloys Compd. 2010;495: 330–3.
22. Gogebakan M, Uzun O, Karaaslan T, Keskin M. Rapidly solidified Al-6.5 wt% Ni alloy. J Mater Process Technol. 2003;142: 87–92.
23. Gang C, Ferry M. Crystallization of Mg-based bulk metallic glass. Trans Nonferrous Met Soc China. 2006;16:833–7.
24. Perez P, Garces G, Gonzalez S, Nitsche H, Sommer F, Adeva P. Change in mechanical properties during crystallization of amorphous $Mg_{83}Ni_9Y_8$. Mater Sci Eng A. 2007;462:211–4.
25. Wolff U, Pryds N, Johnson E, Wert JA. The effect of partial crystallization on elevated temperature flow stress and room temperature hardness of a bulk amorphous $Mg_{60}Cu_{30}Y_{10}$ alloy. Acta Mater. 2004;52:1989–95.